

## Effect of Heat Treatment Temperatures on Microstructure and Corrosion Properties of Inconel 625 Weld Overlay Deposited by PTIG

Longlong Guo<sup>1\*</sup>, Hualin Zheng<sup>1</sup>, Shaohu Liu<sup>2</sup>, Yueqin Li<sup>1</sup>, Chunyu Feng<sup>1</sup>, Xiaodong Xu<sup>1</sup>

<sup>1</sup> School of Mechatronic Engineering, Southwest Petroleum University, Chengdou 610500, PR China

<sup>2</sup> Mechanical Engineering College, Yangtze University, Jingzhou 464023, PR China

\*E-mail: [15108208278@163.com](mailto:15108208278@163.com)

Received: 3 April 2016 / Accepted: 1 May 2016 / Published: 4 June 2016

---

Inconel 625 alloy was cladded on the substrate of AISI 4130 steel using pulsed tungsten inert gas welding (PTIG) technique. The effects of post weld heat treatment (PWHT) temperatures on microstructure evolution and electrochemical corrosion performance of the weld overlay were studied by scanning electron microscopy (SEM), energy dispersive X-ray analysis (EDS) and electrochemical measures. The microstructure of as-welded cladding is mainly composed of  $\gamma$ -Ni columnar grains and precipitates, such as laves and MC. There is no obvious change in microstructure was observed between the rough welded overlay and the overlay after PWHT at 650 °C. With an increase in PWHT temperature, the size of laves phase appear to decrease, and a small number of needle shaped  $\delta$  phase appear in the cladding after PWHT at 750 °C. When the temperature up to 850 °C, a larger number of  $\delta$  phase precipitate at interdendritic regions of the cladding. For PWHT at 950 °C, the  $\delta$  phase coarsens obviously. The electrochemical testing results indicate that heat treatments have noticeable influence on the corrosion parameters, such as charge transfer ( $R_{ct}$ ), self - corrosion potential ( $E_{corr}$ ), pitting potential ( $E_{Pit}$ ), and passivation current density ( $I_p$ ). The higher heat treatments temperature is detrimental to the corrosion resistance, since heat treatments boost the formation of precipitate phase.

---

**Keywords:** Inconel 625; weld overlay; heat treatment; microstructure; corrosion properties

### 1. INTRODUCTION

Inconel 625 as a nickel based alloy exhibits excellent combined performance, for instance favorable mechanical strength, good corrosion resistance, and satisfactory welding workability [1]. The outstanding mechanical properties are mainly depending upon solid-solution strengthening of molybdenum and niobium in austenitic matrix. Additionally, the presence of molybdenum and nickel

provides resistance in non-oxidizing corrosion environment, while chromium and nickel against any form of oxidizing corrosion [2-5]. Owing to above good properties, Inconel 625 has been extensively applied in nuclear power, marine, aeronautical, aerospace, chemical, oil and gas industry. Nevertheless, expensive material cost has seriously limited the bulk application of this alloy [6, 7]. Fortunately, Inconel 625 possesses good ductility, keeping cladding from solidification cracking after welding. So, cladding this alloy on the surface that suffer from aggressive corrosive media is an economical and effective method without comprising corrosion performance of components made from carbon or low alloy steel [1, 5].

It is generally known that cladding is a rapid melting and non-equilibrium solidification process with moving heat source, resulting in high residual stress and even cracks in welds [8]. In working conditions, the residual stress could cause hydrogen induced cracking. Moreover, cracks are harmful to the corrosion resistance, due that cracks play a role as initiations for crevice and pitting damage [3, 9, 10]. Accordingly, proper heat treatments are necessary for cladding to effectively decrease residual stress and adjust microstructure. But the materials of substrate and cladding are dissimilar in chemical composition or mechanical properties. So, its heat treatment is more complicated than the individual alloy or the welding for same material. When determining the heat treatment process for cladding components, combination performance of the cladding and substrate materials should be taking into account.

To date, the reports about Inconel 625 PWHT are mainly concentrated on direct deposited metal to control the formation of laves and the  $\delta$  phase [11-13]. However, very few articles focus on the PWHT for weld overlay of Inconel 625. In this paper, the effects of PWHT temperatures on microstructure evolution and corrosion properties of Inconel 625 weld overlay cladded by PTIG welding technique were investigated, using SEM, EDS and electrochemical measures.

## 2. EXPERIMENTAL DETAILS

### 2.1 Materials and cladding

**Table 1.** Chemical compositions of the materials (Wt. %).

Element	C	Cr	Ni	Ti	Fe	Mo	Al	Nb	Others
AISI 4130	0.29	0.99	0.02	0.006	Bal	0.175	0.006	-	0.72
Inconel 625	0.01	22.65	64.24	0.2	0.32	8.73	0.16	3.53	0.16

The AISI 4130 steel plate having dimensions of 150×150×25mm was used as substrate. It was heat treated with hardening and tempering. The filler wire was nickel based ERNiCrMo-3 (Inconel 625) with 1.2mm diameter. The nominal compositions of the plate and filler wire are shown in Table 1. Working surface of the substrate was grounded with SiC paper and cleaned with acetone to remove oxide and other contaminants. To decrease cold crack in cooling process, plate was preheated to 300 °C in industry furnace, prior to welding.

Fronius automatic PTIG welding system was used to clad Inconel 625 on the substrate. The optimized essential welding parameters used to deposit the cladding are listed in Table 2. The diameters of the jet nozzle and tungsten electrode were 12.5 and 3.2mm, respectively. Pure argon was selected as protecting gas, and flow rate was 15L/min. In a viewpoint of industrial application, two-layer cladding was conducted. This is because that single-layer cladding cannot satisfy the demanded level of corrosion resistance [3, 14]. The length of weld beads was about 125mm and overlap ratio between adjacent welds was 0.4. In cladding processing, temperature of the adjacent tracks was controlled less than 300 °C. After cladding, the specimens cooled naturally to room temperature in air. The macroscopic morphology of Inconel 625 cladding is shown in Fig. 1. It can be observed that top surface of the cladding is relatively smooth and flat. These views also indicated that a good metallurgical bond was formed between cladding and substrate free from cracks or pores.

**Table 2.** Welding parameters used in experiment.

Wire feed rate (m/min)	Welding speed (cm/min)	Preheating current (A)	Peak current (A)	Background current (A)	Frequency (Hz)	Duty cycle
2	18	70	240	90	5	0.3

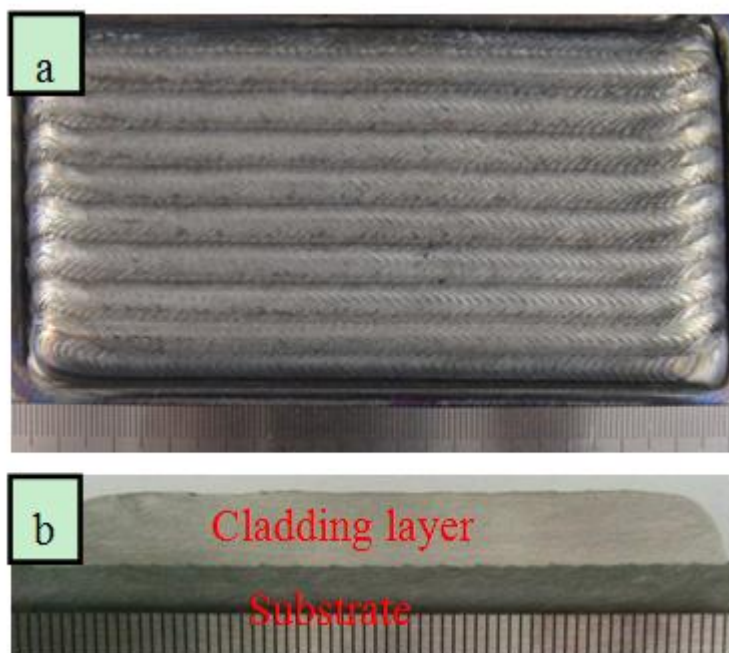


**Figure 1.** Macroscopic morphology of Inconel 625 cladding: (a) top view; (b) cross sectional view.

The specimens used to estimate the effects of PWHT on the microstructure and corrosion resistance were machined by wire cutting to obtain a surface and the eventually distance between the substrate working surface was about 5.9 mm. The composition analysis results of the cladding surface are presented in Table 3. Then, the cladding sample was divided into five parts. One was selected as

welded sample and marked A. While other samples were treated with two hours hold time at 650, 750, 850 and 950 °C, respectively. And, the corresponding samples were marked B, C, D and E, respectively. After heat treating, the samples were cooled in air to room temperature.

**Table 3.** Chemical compositions of the cladding surface (Wt. %).

Element	Si	Cr	Ni	Ti	Fe	Mo	Al	Nb
Cladding	0.23	22.21	63.22	0.17	2.01	8.34	0.12	3.34

## 2.2 Characterization techniques

The metallographic specimens were prepared according to standard metallographic procedures and electrolysis etched using a mixture solution (12 mL H<sub>3</sub>PO<sub>4</sub> + 40 mL HNO<sub>3</sub> + 48 mL H<sub>2</sub>SO<sub>4</sub>) at 6 V about 15 s to reveal the microstructure. The microstructures of the samples were first observed using an SDPTOP RX50M optical microscopy. Further microstructural study was conducted using a JSM-6490LV SEM.

## 2.3 Electrochemical tests

Each specimen was jointed to a copper conductive wire by welding and then it was mounted with epoxy resin, remaining a surface with 100mm<sup>2</sup> used as testing surface. For the sake of test accuracy, the testing surface was prepared using metallographic procedures to guarantee consistent surface roughness. A 3.5 wt.% NaCl solution prepared with de-ionized water was used to electrochemical tests at room temperature. Prior to testing, the specimens were cleaned by ultrasonic in acetone, following rinsed in distilled water, and dried in air. The electrochemical measurements were conducted using a standard three electrode cells, in which platinum plate working as counter electrode, and saturated calomel electrode (SCE) used as electrode.

Electrochemical impedance spectroscopy (EIS) and potentiodynamic polarization were tested using an Autolab (PGSTAT302N) to evaluate electrochemical behavior of the Inconel 625 weld overlay. Before all corrosion measurements, specimen was held at its rest potential to reach a stable open-circuit potential. The EIS testing was performed at open circuit potential of the specimen in a frequency range from 10KHz to 0.01 Hz, with amplitude of 10 mV. The ZsimpWin software was used to fit the EIS data. Potentiodynamic polarization were measured based on the guideline in ASTM standards G5-94 and G61-86. So, the tests scans were performed from open circuit potential at a scan rate of 20 mV /min. The potential range was -200 to 1500 mV.

## 3. RESULTS AND DISCUSSION

### 3.1 Microstructures of cladding under various PWHT

The microstructure of the weld overlay in rough welding condition is mainly composed of columnar grains, as shown in Fig. 2. It is also observed that a great number of white irregular shaped

and some tetragonal particles phases existed in interdendritic spaces. Table 4 presents EDS results of the precipitate phases. It can be found that primary hardening and corrosion resistant elements Nb and Mo are significantly richer in irregular shaped phase when compared with the matrix. Moreover, chemical compositions of this phase approximately accord with  $A_2B$  (A: Ni, Fe, Cr; B: Nb, Mo, Ti) type phase [15]. Therefore, the irregularly shaped phase was identified as laves phase. The square shaped precipitates are rich in C, Nb and Ti, and it could be MC (NbC and TiC) [16].

The formation of precipitates is mainly caused by the segregation of alloy elements. In the cladding process, the solidification of melt pool initiate with the reaction  $L \rightarrow \gamma$ , inducing the elements Nb, Mo and C are rejected to the liquid in the intergranular spaces. The accumulation of these elements boosts the reaction  $L \rightarrow \gamma + MC$ , which occupies a mass of available C. With a further solidification, the concentration of alloy elements becomes more serious. Finally, laves phase forms by the reaction  $L \rightarrow \gamma + MC + laves$ , finishing the solidification process. It can be seen that the formation of laves depletes most of useful elements. Particularly, the content of Nb in laves phase is up to 17.28%, resulting in poor tensile ductility, fracture toughness and corrosion resistance.

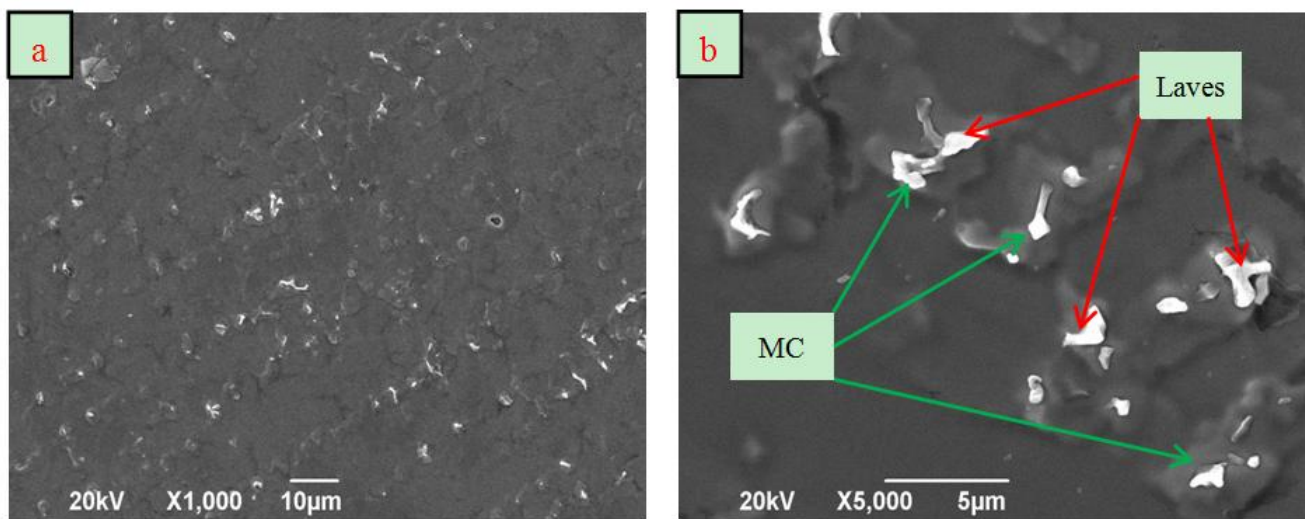


**Figure 2.** SEM images of the major phases in microstructure of weld overlay: (a) low magnification; high magnification.

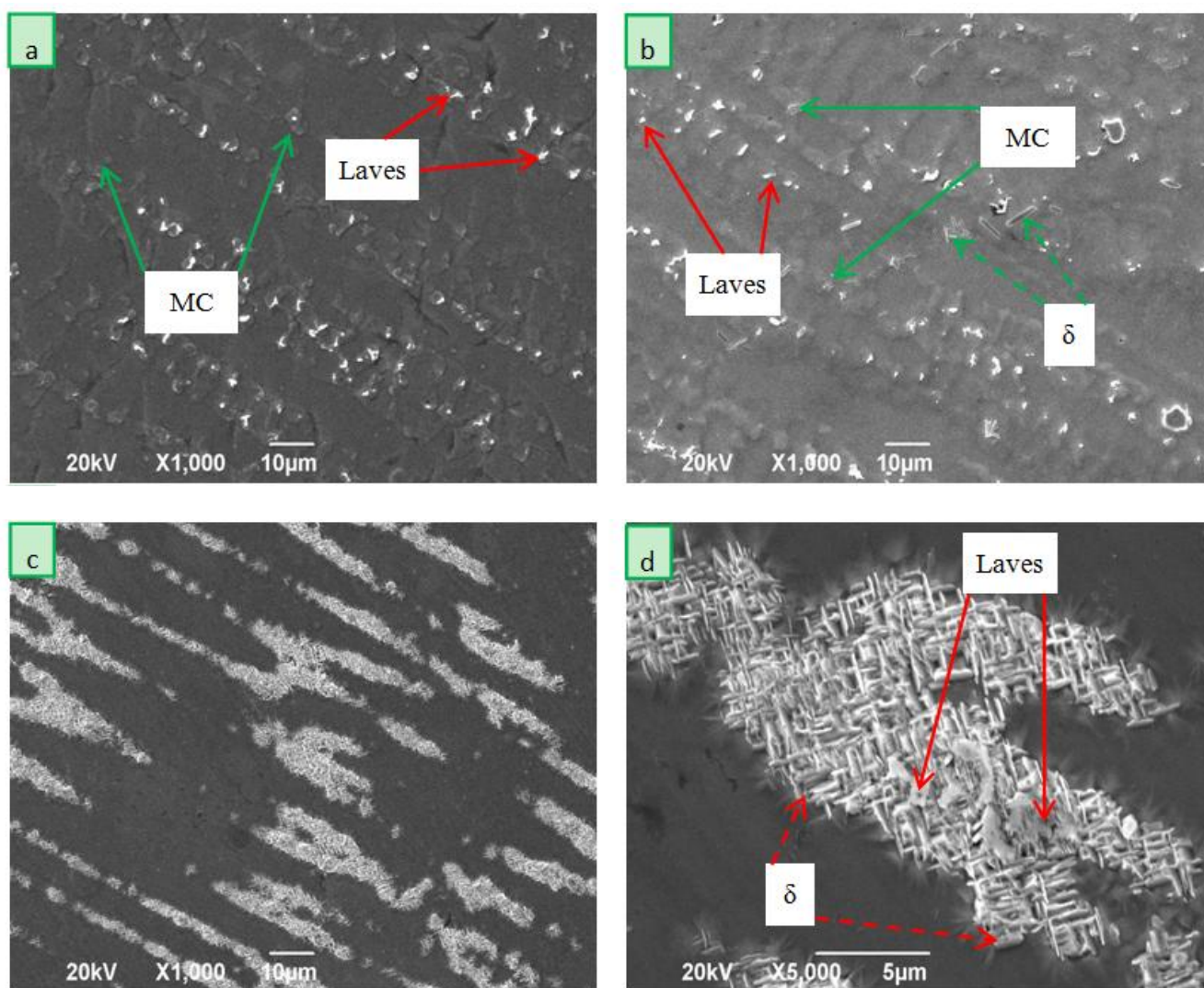
**Table 4.** Compositions of matrix and precipitates in microstructure of weld overlay (Wt. %).

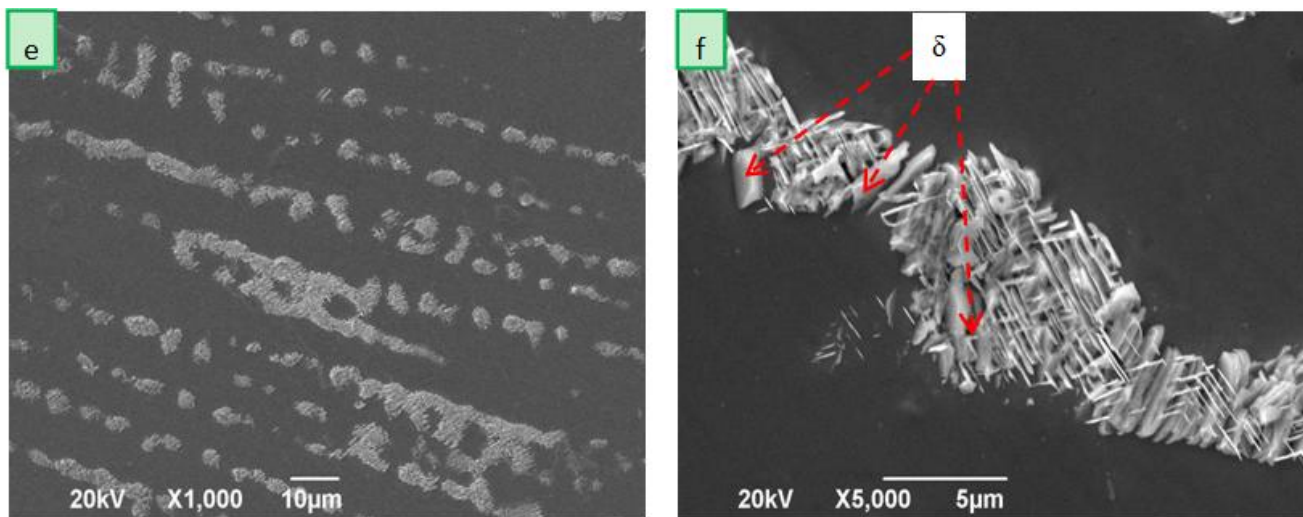
Phases	C	Nb	Mo	Ti	Cr	Fe	Ni
Matrix	-	3.04	8.33	0.38	22.21	2.01	64.03
Laves	-	17.28	14.41	0.58	17.55	1.37	48.81
MC	8.88	52.05	8.91	2.69	7.74	2.73	17.01

Fig.3 presents the SEM images of the cladding under various heat treatments process. Compared with the rough welded condition, there is no evidence that the microstructure of the

cladding after PWHT at 650 °C changes obviously, besides the number and dimensions of the secondary phases seem to increase. With an increase in PWHT temperature, the size of laves phase appear to decrease, and a small number of needle shaped phase appear in the microstructure after PWHT at 750 °C. This phase features three different orientations. So, depending upon its orientation characters, this needle shaped phase could be  $\delta$  [ $X_3M$ ] phase. This result is consistent with the morphological observation study by previous researchers [11, 17, 18]. The chemical compositions of the  $\delta$  phase are listed in Table 5. It is found that besides Ni and Nb, there are large amounts of other elements, such as Cr, Al, Fe and Ti, in this phase. Cozar, R [19] and M. Sundararanan [20] have pointed out that nickel in the  $\delta$  phase can be partially replaced with Fe and Cr, and that Nb atomic would be partially substituted by Ti and Al. These also go some way to explaining the large amounts distribution of the  $\delta$  phase.

The evolution of microstructure is mainly because that temperature has rapidly positive influence on diffusion rate and solution solubility of the elements in  $\gamma$ -Ni matrix. With an increase in PWHT temperature, the size and content of laves gradually decline.





**Figure 3.** SEM micrographs of the cladding after different heat treatments: (a) 650 °C; (b) 750 °C; (c, d) 850 °C; (e, f) 950 °C.

Thereby, a mass of Nb element was released in the interdendritic spaces, providing beneficial conditions for the formation of  $\delta$  phase. When the PWHT temperature up to 850 °C, a large number of  $\delta$  phase exhibiting net distribution were precipitated in the interdendritic regions with only a small number of laves residual. After PWHT at 950 °C, the  $\delta$  phase coarsens notable with the number of  $\delta$  phase decrease. But, some fine  $\delta$  phase can be observed near the rod shaped  $\delta$  phase. The formation of  $\delta$  phase consuming a lot Ni and Nb elements could result poor corrosion resistance.

**Table 5.** Chemical compositions of phases precipitated in the microstructure of Inconel 625 cladding after PWHT (Wt. %).

Phases	Nb	Mo	Ti	Cr	Fe	Ni
$\delta$	12.31	10.60	0.59	17.72	1.44	56.80

### 3.2 Effect of PWHT on the corrosion resistance

#### 3.2.1 Electrochemical impedance spectroscopy

The EIS plots of as-welded and various treated Inconel 625 weld overlay at their open-circuit potential are shown in Fig.4. All Nyquist plots feature single capacitive loop, but differ in diameter. These indicate that corrosion processing was controlled by electrochemical reaction [21]. Only one time constant is observed for each bode curve. The equivalent circuit model used to fit the EIS data is expressed in Fig.5. In the model,  $R_s$  and  $R_{ct}$  correspond to the solution resistance and charge transfer resistance, respectively. The larger the  $R_{ct}$  value is, the better corrosion resistance of the sample is expected [22]. In consideration of rough surface, double layer capacitance was denoted by a constant phase element (*CPE*) to obtain a more accurate fitting. In addition, the value of  $n$  in the *CPE* reflects

the surface characters. When  $n$  is close to 1, it means that the weld overlay is smooth and the passive layer is compact and homogeneous. But, When  $n$  is far away from 1, it suggests that the weld overlay is rough and more corroded reflecting poor corrosion resistance.

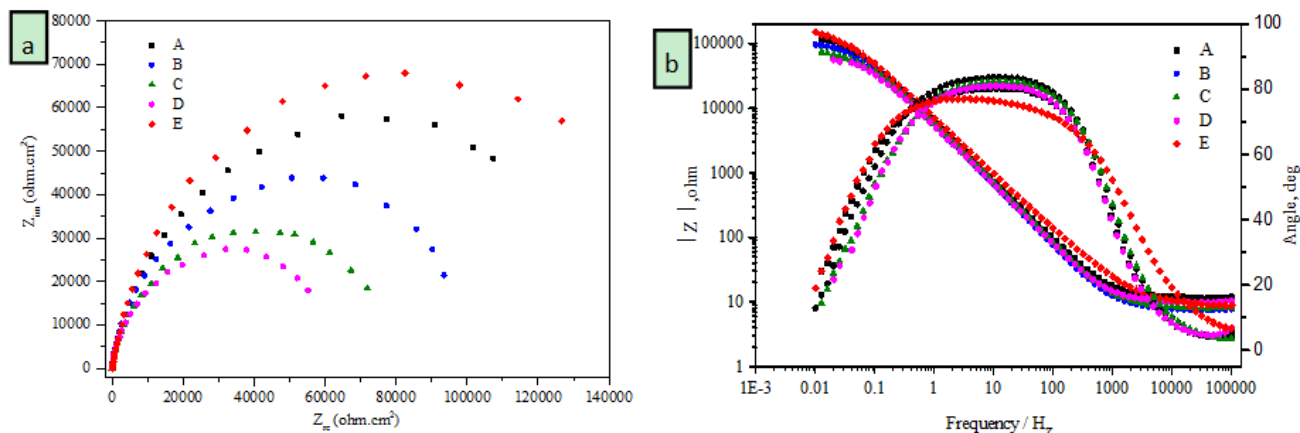


**Figure 4.** EIS results of Inconel 625 overlay cladding under various heat treatment conditions: (a) Nyquist impedance; (b) Bode plots.

The corresponding values of various components determined by ZsimpWin are listed in Table 6, and the fitting errors for each plot were smaller than 5%. From the table, it can be found that fluctuations of  $R_s$  for different specimen are not remarkable, indicating that the measure system is under stable conditions for each testing. The charge transfer resistance  $R_{ct}$  of the specimens  $B$ ,  $C$  and  $D$  are lower than that of the rough welded specimen  $A$ . But, the specimen  $E$  exhibits the largest  $R_{ct}$  values in all specimens. In electrode reaction process, the values of  $R_{ct}$  reflect the resistance of the charge through electrical double layer between the electrode and electrolytic-solution. Generally, the higher  $R_{ct}$  value suggests that transport process of charge is relative difficult. In other words,  $R_{ct}$  is a positive indicator for corrosion resistance. Therefore, the  $R_{ct}$  value of the specimens treated at various temperatures demonstrate that heat treatments at 650 °C, 750 °C and 850 °C for 2 h are bad for corrosion resistance of the Inconel 625 weld overlay. On the contrary, heat treatment at 950 °C is benefit to the corrosion resistance of the weld overlay.

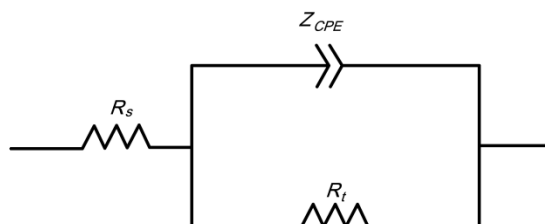


**Figure 5.** Equivalent circuit model corresponding to the Nyquist plots of various heat treated Inconel 625 weld overlay.

**Table 6.** Fitting parameters for EIS results of Inconel 625 weld overlay.

Specimens	$R_s (\Omega \text{ cm}^2)$	$Q$		$R_{ct} (\Omega \text{ cm}^2)$
		$Y_0 (\Omega^{-1} \text{ cm}^{-2} \text{ S}^n)$	$n$	
A	10.661	3.176E-05	0.904	1.33E5
B	8.701	3.255E-05	0.929	9.65E4
C	8.245	3.232E-05	0.916	7.39E4
D	8.002	2.627E-05	0.912	6.13E4
E	9.332	2.918E-05	0.852	1.77E5

3.2.2 Potentiodynamic polarization

The potentiodynamic polarization curves of the all specimens in 3.5% NaCl solution are shown in Fig.6. It is clear that the overlay cladding of Inconel 625 heat treated at 650 °C, 750 °C and 850 °C show a relative stable passivation stage, where the current density is irrelevant to the applied potential. Moreover, there is no obvious fluctuation of current density with the increasing of potential in the passivation region. But for the as-welded specimen and specimen treated at 950 °C, the current densities change back and forth with the increase in potentials applied, following by a narrow passivation zone. These indicate that the protective film was damaged and the repassivation behavior occurs. According to above results, it can be concluded that heat treatments at 650 °C, 750 °C and 850 °C for 2 h can widen the passivation region and enforce the stability of passive layer formed on the overlay cladding.

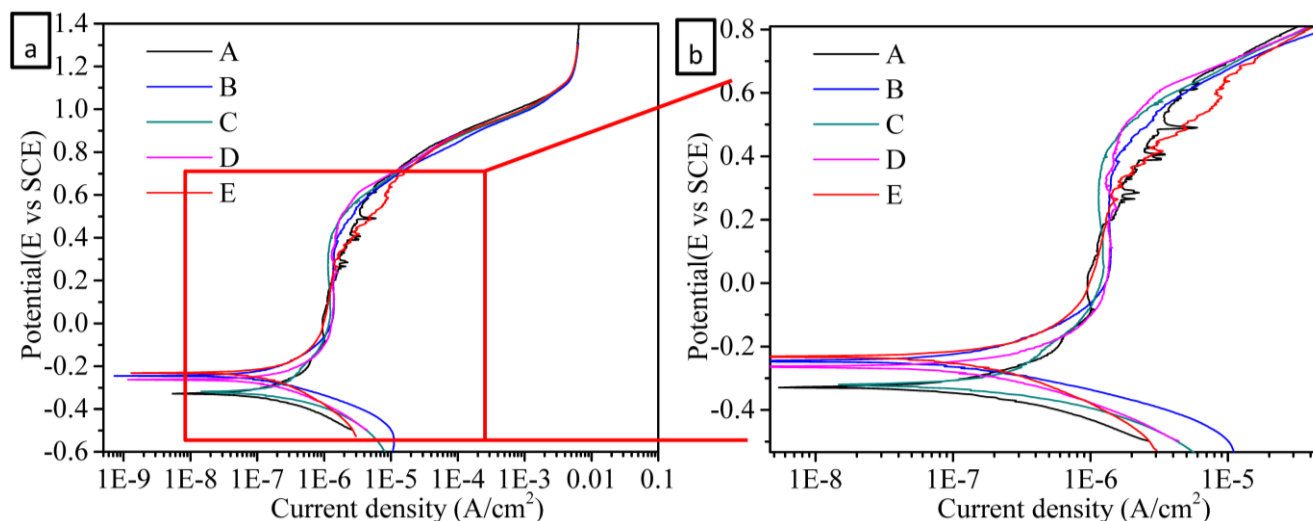


**Figure 6.** Polarization curves of cladding under various heat treatments in 3.5% NaCl solution: (a) overall view of polarization curves; (b) magnified view of the overlapped region.

In potentiodynamic polarization curves analysis of a material, the self-corrosion potential ( $E_{corr}$ ), pitting potential ( $E_{pit}$ ), and passivation current density ( $I_p$ ) are primary parameters in evaluation

of corrosion performance [3]. Generally, the value of  $E_{corr}$  represents the corrosion susceptibility. So, the nobler  $E_{corr}$  means that a material is difficult to initiate corrosion. The  $E_{pit}$  reflects the resistance against occurrence of local damage on the protective film [23]. The higher  $E_{pit}$  suggests that permanent damage cannot occur at the passive film, when low electrochemical voltages applied. Formation of protective layer at a low passivation current density can effectively prevent further corrosion at higher current densities [24]. So, the  $I_p$  is regard as a positive indicator for uniform corrosion resistance.

The corresponding corrosion parameters were determined from the curves and displayed in Fig.7. The corrosion potential ( $E_{corr}$ ) was found to follow the sequence:  $E > B > D > C > A$ . It indicates that the smallest driving force was required to initiate the corrosion of the as-welded cladding. That is to say, the as-welded specimen is vulnerable to initiate corrosion. It is also observed that Pitting potential ( $E_{pit}$ ) values of these specimens with the order:  $A > D > B > C > E$ . This result declares that the rough welded specimen exhibits better resistance to pitting corrosion. In addition, the passivation current density ( $I_p$ ) is following the sequence:  $A < C < D < B < E$ , indicating that heat treatment is impairment to the formation of passivation layer.

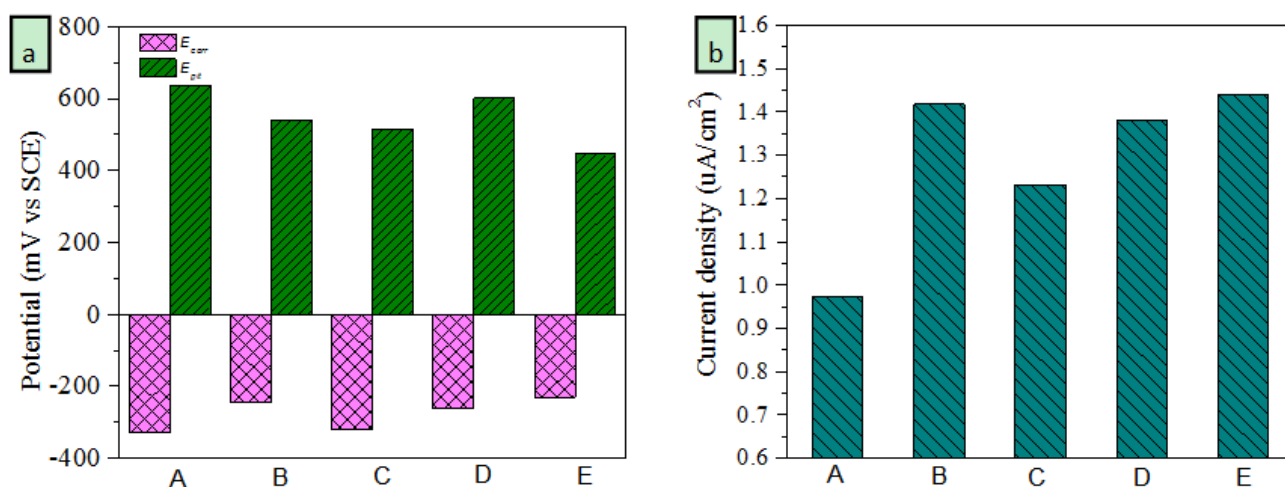


**Figure 7.** Corrosion parameters of Inconel 625 overly under different heat treated states: (a) corrosion and pitting potentials; (b) passivation current density.

### 3.2.3 Surface morphology of the cladding after electrochemical testing

The surface morphology images of the various heat treatments weld overlay after potentiodynamic polarization testing are shown in Fig.8. For the all specimens, there is no obvious feature of the pits throughout the testing surface. It can be inferred that the pitting damage does not occur during the testing processing. This phenomenon accords with the results that the gradients of the current density against potential are very low in the transpassive regions. The amount and density of corrosion products formed on the corroded surface of the specimens seems to decrease with the temperature of heat treatments. Particularly, only very little corrosion products distributed on the dendritic matrix of the specimen treated at 850 °C and 950 °C. The decrease in amount and density of

corrosion products reflects the degenerated corrosion resistance [25]. Moreover, it can be found that the morphology or abundance of the precipitates changes not significant.

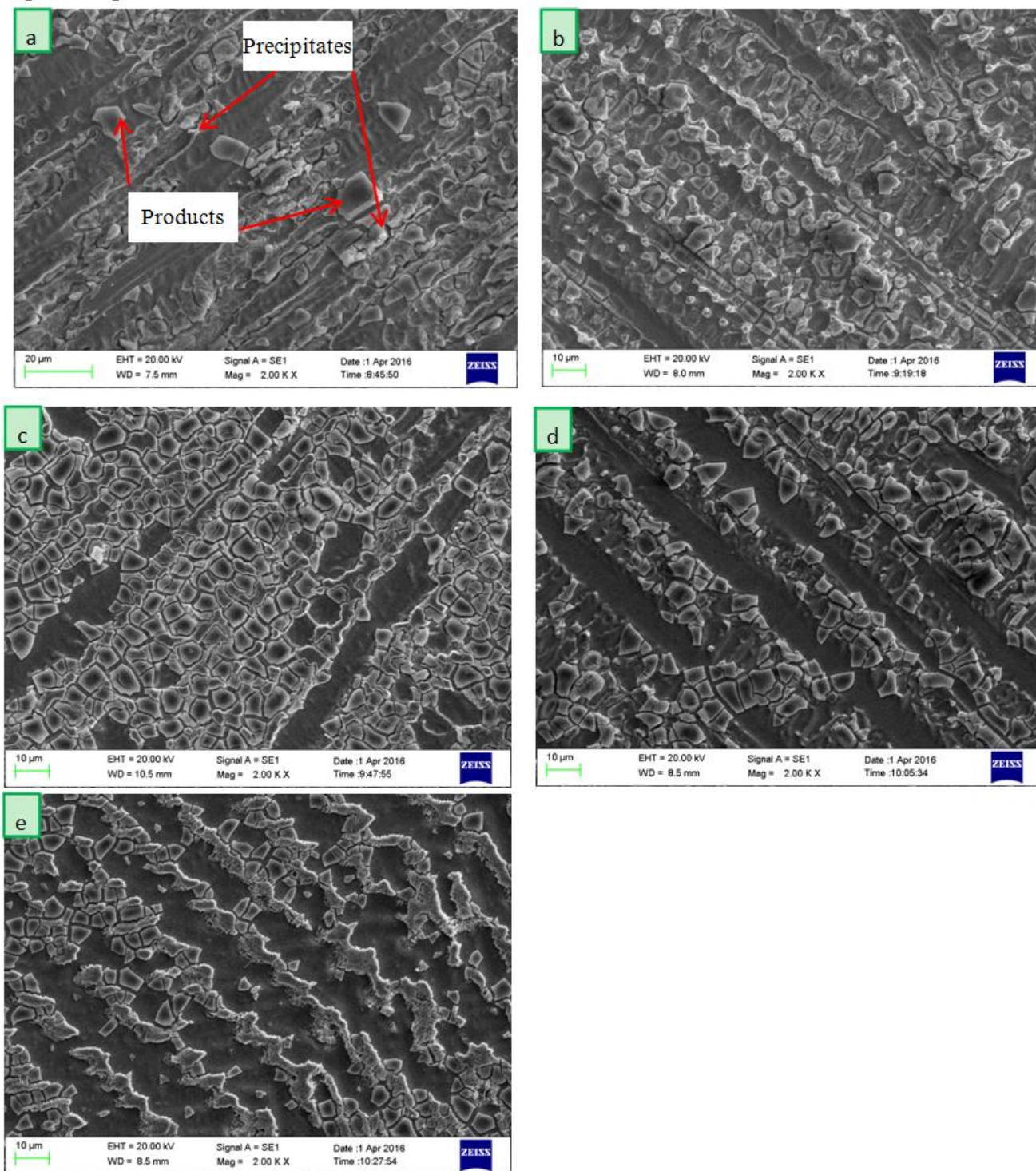


**Figure 8.** Surface morphology of the specimens after potentiodynamic polarization test: (a), (b), (c), (d), (e) represent specimen A, B, C, D, and E, respectively.

According to the above description, the corrosion mechanism is believed to be in form of galvanic coupling. And, the dendritic matrix plays a role as sacrificial anode, since it was preferentially corroded. During the heat treatments process, elements of Cr, Nb and Mo diffuse from dendrite cores to interdendritic, increasing the chance of precipitates phase development in interdendritic regions [26]. Additionally, the diffusion rates of elements rapidly increase with the temperature. Therefore, higher temperature of heat treatments could cause more serious segregation of elements in the interdendritic. Due to the poor corrosion resistant elements region in the vicinity of precipitates boundary, the potential of the grain boundary changes more negative. So, these regions are vulnerable to initiate corrosion. Moreover, serious corrosion damage could occur when the content of Cr and Mo is less than the critical value [27, 28]. Therefore, heat treatments could heighten the segregation of the Inconel 625 cladding, boosting the formation of precipitate phase, and spoiling corrosion resistance.

#### 4. CONCLUSIONS

The influences of heat treatments on the microstructure and corrosion performance of the Inconel 625 weld overlay have been investigated and the following main conclusions can be attained:

(1) The microstructure of the weld overlay in rough welding condition is primarily composed of columnar grains and precipitates such as laves and MC phases in the interdendritic regions. There is no obvious change in microstructure was observed between the rough welded overlay and the overlay after PWHT at 650 °C. With an increase in PWHT temperature, the size of laves phase appear to decrease, and a small number of needle shaped  $\delta$  phase appear in the cladding after PWHT at 750 °C. When temperature up to 850 °C, a larger number of  $\delta$  phase precipitate at interdendritic regions of the cladding. For PWHT at 950 °C, the  $\delta$  phase coarsens obviously.

(2) All rough and heat treated weld overlay of Inconel 625 exhibit a depressed semicircle but differ in diameter. When the temperature below 850 °C, the value of charge transfer resistance ( $R_{ct}$ ) decrease with the increase in temperature of heat treatments. Moreover, the sample heat treated at 950 °C shows the largest charge transfer resistance ( $R_{ct}$ ).

(3) The testing specimens show a passive behavior in anion polarization. The as welded cladding features larger pitting corrosion ( $E_{pit}$ ), and lower passivation current densities ( $I_p$ ). But, the specimen heat treated at 950 °C is harder to initiate corrosion, because of larger corrosion potential ( $E_{corr}$ ).

(4) The corrosion mechanism is believed to be in form of galvanic coupling. And, the dendritic matrix plays a role as sacrificial anode. During the heat treatments process, elements of Cr, Nb and Mo diffuse from dendrite cores to interdendritic. Therefore, heat treatments at high temperature boost the formation of precipitate phase, and spoiling corrosion resistance.

#### ACKNOWLEDGEMENT

The authors would like to thank the Innovation Foundation of Southwest Petroleum University (CX2014BY05) and Open Foundation of Education Department Key Laboratory of Oil and Gas Equipment (OGE201401-01) for sponsoring this study. The authors also gratefully acknowledge the Chongqing Xintai Petroleum Machinery Company for support of the cladding experiment.

## References

1. T.E. Abioye, D.G. McCartney and A.T. Clare, *J. Mater. Process. Tech.*, 217(2015) 232.
2. S. Li, Q. Wei, Y. Shi, Z. Zhu and D. Zhang, *J. Mater. Sci. Technol.*, 31(2015) 946.
3. H.R. Zareie Rajani, S.A.A. Akbari Mousavi and F. Madani Sani, *Mater. Design*, 43(2013) 467.
4. Z.F. Yin, W.Z. Zhao, W.Y. Lai and X.H. Zhao, *Corros. Sci.*, 51(2009) 1702.
5. L.Y. Xu, M. Li, H.Y. Jing and Y.D. Han, *Int. J. Electrochem. Sc.*, 8(2013) 2069.
6. T.E. Abioye, J. Folkes and A.T. Clare, *J. Mater. Process. Tech.*, 213(2013) 2145.
7. C.C. Silva, H.C.D. Miranda, M.F. Motta, J.P. Farias, C.R.M. Afonso and A.J. Ramirez, *Journal of Materials Research and Technology*, 2(2013) 228.
8. J. Cao, F. Liu, X. Lin, C. Huang, J. Chen and W. Huang, *Optics & Laser Technology*, 45(2013) 228.
9. S. Zhou, Y. Huang, X. Zeng and Q. Hu, *Materials Science and Engineering: A*, 480(2008) 564.
10. F. Madadi, M. Shamanian and F. Ashrafizadeh, *Surface and Coatings Technology*, 205(2011) 4320.
11. F. Xu, Y. Lv, Y. Liu, B. Xu and P. He, *Physics Procedia*, 50(2013) 48.
12. G.P. Dinda, A.K. Dasgupta and J. Mazumder, *Materials Science and Engineering: A*, 509(2009) 98.
13. X. Xing, X. Dia and B. Wang, *J. Alloy. Compd.*, 593(2014) 110.
14. J.S. Kim, Y.I. Park and H.W. Lee, *Met. Mater. Int.*, 21(2015) 350.
15. F. Xu, Y. Lv, Y. Liu, F. Shu, P. He and B. Xu, *J. Mater. Sci. Technol.*, 29(2013) 480.
16. K.H. Song and K. Nakata, *Mater. Design*, 31(2010) 2942.
17. W.R. Sun, S.R. Guo, J.H. Lee, N.K. Park, Y.S. Yoo, S.J. Choe and Z.Q. Hu, *Materials Science and Engineering: A*, 247(1998) 173.
18. D. Zhang, W. Niu, X. Cao and Z. Liu, *Materials Science and Engineering: A*, 644(2015) 32.
19. R. Cozar and A. Pineau, *Metallurgical Transactions*, 5(1974) 2471.
20. M. Sundararaman, P. Mukhopadhyay and S. Banerjee, *Metallurgical Transactions A*, 23(1992) 2015.
21. B.T. Ter-Ovanesian, C. Alemany-Dumont and B. Normand, *Electrochim. Acta*, 133(2014) 373.
22. J.L. Trinstancho-Reyes, M. Sanchez-Carrillo, R. Sandoval-Jabalera, V.M. Orozco-Carmona, F. Almeraya-Calderon, J.G. Chacon-Nava, J.G. Gonzalez-Rodriguez and A. Martinez-Villafane, *Int. J. Electrochem. Sc.*, 6(2011) 419.
23. A. Mortezaie and M. Shamanian, *Int. J. Pres. Ves. Pip.*, 116(2014) 37.
24. H.R.Z. Rajani, S.A.A.A. Mousavi and F.M. Sani, *Mater. Design*, 43(2013) 467.
25. T.E. Abioye, P.K. Farayibi, D.G. McCartney and A.T. Clare, *J. Mater. Process. Tech.*, 231(2016) 89.
26. S. Chaudhari and P.P. Patil, *Electrochim. Acta*, 56(2011) 3049.
27. C. Chen, R. Jiang, G. Zhang, S. Zheng and L. Ge, *Rare Metal Mat. Eng.*, 39(2010) 427.
28. W. Tian, F. Xie and X. Zhao, *Rare Metal Mat. Eng.*, 41(2012) 482.